Mon. Not. R. astr. Soc. (1983) **202,** 495–510

Inverse Compton gamma-rays from pulsars – I. The Vela pulsar

Marco Morini *Istituto di Fisica Cosmica e Informatica del CNR, via Archirafi, 36, I-90123, Palermo, Italy*

Received 1982 May 3; in original form 1982 March 8

Summary. A model is proposed for pulsar optical and gamma-ray emission where relativistic electrons beams: (i) scatter the blackbody photons from the polar cap surface giving inverse Compton gamma-rays and (ii) produce synchrotron optical photons in the light cylinder region which are then inverse Compton scattered giving other gamma-rays. The model is applied to the Vela pulsar, explaining the first gamma-ray pulse by inverse Compton scattering of synchrotron photons near the light cylinder and the second gamma-ray pulse partly by inverse Compton scattering of synchrotron photons and partly by inverse Compton scattering of the thermal blackbody photons near the star surface.

1 Introduction

Among the 25 gamma-ray sources of the 2CG catalogue published by the Caravane Collaboration for the *COS-B* satellite (Swanenburg *et al.* 1981) only two, the Crab and Vela pulsars (Bennett *et al.* 1977; Kanbach *et al.* 1980), have been unambiguously identified with point sources. A search for gamma-ray emission from other radio pulsars has been performed in the data of the *SAS-2* and *COS-B* satellites. Indication of pulsed gamma-ray emission was reported for the *SAS-2* data in the case of PSR 1747 – 46 and 1818 – 04 (Ögelman *et al.* 1976). However, the chance of a positive observation in the case of PSR 1747 – 46 and 1818 – 04 seems very improbable because the reported luminosities exceed the rotational energy loss $\dot{E} = I\Omega\dot{\Omega}$ of these pulsars 50 and 20 times respectively (for the radio timing data see Newton, Manchester & Cooke 1981). As a preliminary result of the *COS-B* data analysis the possibility of pulsed gamma-ray emission from PSR 0740 + 28 and 1822 – 09 has been suggested (Pinkau 1979), but the situation is not clear: at the location of each of the two pulsars is found an excess of counts consistent with that derived from the timing analysis, but the observed gamma-ray periods are not in agreement with the contemporary radio periods (Buccheri 1981). Also the detection of soft gamma-ray (< 1 MeV) pulsed emission from PSR 1822 – 09 has been reported (Mandrou, Vedrenne & Masnou 1980).

That being the case, the only data we can reliably use about pulsar gamma-ray emission are the Crab and Vela ones. For the Crab pulsar satisfactory models for the optical, X- and gamma-ray emission exist. They are based on synchrotron emission from electrons and positrons in a region of plasma instability above the magnetic polar caps, near the speed of

light cylinder radius (Zheleznyakov & Shaposhnikov 1972; Hardee 1979; Machabeli & Usov 1979). These models can be adapted to the models of Arons & Scharlemann (1979) or Jones (1980) for the particle acceleration and pair creation in a $\mathbf{\Omega}\cdot\mathbf{B}>0$ pulsar magnetosphere (with $\mathbf{\Omega}$ the angular velocity and $\mathbf{B}$ the magnetic field) or to that of Ruderman & Sutherland (1975) for a $\mathbf{\Omega}\cdot\mathbf{B}<0$ pulsar. However, because of the drastic dependence of the gamma-ray luminosity on the period ($L_\gamma \propto \Omega^4$) characteristic of these synchrotron models, they do not predict a strong gamma-ray emission from slower pulsars. Actually, for the Vela pulsar, synchrotron emission near the speed of light cylinder is unlikely to reach the high energy side of the gamma-ray band. Thompson (1975) gives an upper limit to the synchrotron spectrum of about $\epsilon_{\max} = 180\,\mathrm{MeV}$ for $\gamma = 4\times10^6$ electrons in a $B_\perp = 10^3\,\mathrm{G}$ magnetic field, using the Shen (1972) expression

$$\epsilon_{\max} = 1.2\times10^{-8}\gamma^2 B\ \mathrm{eV}. \tag{1}$$

As the Vela gamma-ray spectrum has been observed to extend at least up to $\epsilon_{\max} = 2\,\mathrm{GeV}$ (Kanbach *et al.* 1980) we require $\gamma = 1.5\times10^7$ electrons at the light cylinder radius. These electrons are very efficiently converted into curvature gamma-rays near the star surface, where therefore we expect gamma-ray emission rather than at the speed of light cylinder (see for instance Salvati & Massaro 1978).

The current models for the pulsar gamma-ray emission are via vacuum discharge and curvature radiation near the neutron star surface (Hardee 1977; Massaro & Salvati 1979; Harding 1981; Ayasli 1981). As a matter of fact, however, no detailed attempt has been made to date to explain within these models all the observational data about gamma-ray pulsars. So, there is no doubt that magnetic limited vacuum gaps can develop near the pulsar polar cap surface, but it appears unlikely that the resulting curvature gamma-ray emission can account for the observed double peaked gamma-ray light curves and for the high energy side ($>1\,\mathrm{GeV}$) of the spectrum. Outer gap models (Cheng, Ruderman & Sutherland 1976; Ayasli & Ögelman 1980; Ray & Benford 1981) might reproduce the observed gamma-ray light curves, but present other difficulties, which will be considered with some detail in the next section.

Here an inverse Compton model is proposed for the optical, X- and gamma-ray pulsar emission. The model is applied to the Vela pulsar to describe the details of the observational data, such as luminosities, light curves and spectral differences between the two gamma-ray pulses. A particle distribution in the magnetosphere consistent with the Ruderman & Sutherland (1975) model for the $\mathbf{\Omega}\cdot\mathbf{B}<0$ pulsar magnetosphere is assumed. The basic idea is to have high-energy photons produced by inverse Compton scattering of relativistic electrons with: (i) thermal X-ray photons from the hot polar cap surface (Morini 1981), giving most of the second pulse gamma-ray emission; and (ii) synchrotron optical and soft X-ray photons emitted by the same scattered electrons (synchro-Compton emission) in the light cylinder region, producing the optical emission and in the gamma-ray band the first pulse and part of the second pulse emission. Synchro-Compton emission has been first considered in the pulsar context by Zhelezynakov & Shaposhnikov (1972) in their model for the Crab pulsar emission. Comparing their analytical results with the Crab *COS-B* gamma-ray spectrum (Lichti *et al.* 1980) we can infer that inverse Compton emission is not necessary to explain the gamma-ray spectrum in the case of the Crab pulsar. Inverse Compton scattering has been also considered by Schlickeiser (1980) to explain the 1 GeV cut-off in the first reported gamma-ray spectra of the Crab and Vela pulsars (Bennett *et al.* 1977) as a result of the high-energy reduction of the Klein–Nishina cross-section, suggesting electron distributions of the form $N(E)\propto E^{-p}$ with $p\simeq 2.6$ and 1.6 for the Crab and Vela pulsars and target photons energies $\epsilon\simeq 10\,\mathrm{keV}$ and 1 keV, respectively. However, improved analyses of the gamma-ray data have shown that the gamma-ray power-law spectra actually extend up

to higher energies than first reported (Lichti *et al.* 1980), so that the results from Schlickeiser (1980) cannot be directly applied.

This work refers mainly to the Vela pulsar. Faster or slower pulsars will be considered in a further paper. Section 2 is concerned with the discussion of the emission region location, starting from the consideration of the radio, optical and gamma-ray pulse profile of the Vela pulsar emission. It is shown that a simple way to explain the light curves is to assume that the optical and gamma-ray emission derives from particles moving along the magnetic field lines in the open part of the magnetosphere above one polar cap, near the edge of the close corotating magnetosphere, at a distance from the star surface about 0.5 and 0.7, respectively, in light cylinder radius units, together with gamma-ray emission near the polar cap surface, while the radio emission is produced near the star surface above the other polar cap. Concluding the discussion on the emission regions the proposed outer gap models are considered with some detail.

In Section 3 the inverse Compton emission mechanisms both near the star surface and in the light cylinder region are described, giving the complete set of equations which has been used for the calculations. Section 4 presents the results of the computer calculation for the Vela pulsar, giving the spectra and the light curves in the different energy bands for a parameter choice which well describes the observational data.

Throughout this work an orthogonal pulsar geometry with a dipolar magnetic field in the corotating frame is assumed, supposing that the differences in the observed radiation from the two different polar caps are due to the observer not lying exactly in the pulsar equatorial plane.

2 Location of the emission regions

It seems well proved that the Vela radio emission is produced deep inside the magnetosphere of the pulsar, near the neutron star surface. The stronger evidence, reported by Radhakrishnan & Cooke (1969) and Davila, Wright & Benford (1980), is that the radio emission is highly polarized with the direction of polarization sweeping through an angle of 90° during the duration of the pulse, which has a very small angular width (~10°). The simpler way to explain this fact is that the radio emission is curvature radiation from the inner part of the open magnetosphere, where the planes of the magnetic field lines have not yet diverged more than the observed pulse width.

The optical and gamma-ray light curves are more complicated than the radio one. In the gamma-ray band we have two pulses, with a relative separation 0.41 in phase, the first pulse at a phase $\phi = 0.12$ with respect to the radio peak (Kanbach *et al.* 1980; Buccheri *et al.* 1978). The second gamma-ray pulse presents a harder spectrum than the first one (Kanbach *et al.* 1980). In the optical band the two pulses have a relative separation 0.25 in phase and are located within the two gamma-ray pulses (Wallace *et al.* 1977; Manchester *et al.* 1980).

Different explanations have been invoked to account for the phase separation of ~150° in the gamma-ray band, in the hypothesis that the two pulses derive from the two opposite polar caps: for example, a distorted magnetic field geometry (Thompson 1975; Hardee 1979), or a hollow cone asymmetric geometry (Massaro, Salvati & Buccheri 1979). Moreover, as advanced in the introduction, outer gap geometries have been proposed to explain the pulse–interpulse separation in the gamma-ray pulsar emission (Cheng *et al.* 1976; Cheng & Ruderman 1977; Ayasli & Ögelman 1980; Ray & Benford 1981). Outer gap models present a basic difficulty. The original Holloway (1973) idea was that in the *closed* corotating part of the magnetosphere, where the force-free charge density ρ is given by

$$\rho = -\frac{\boldsymbol{\Omega}\cdot\mathbf{B}}{2\pi c}\left\{1-\left(\frac{\Omega r}{c}\sin\theta\right)^2\right\}^{-1} \qquad (2)$$

with θ the magnetic colatitude and r the distance from the star (Goldreich & Julian 1969; Mestel 1971), if we have complete charge separation as expected for particles deriving from the star surface, then the $\boldsymbol{\Omega}\cdot\mathbf{B}=0$ surface is a null mass density surface as well as a null charge density surface and is unstable against depleting perturbations because the magnetic field lines cross it. A vacuum gap can therefore grow around this $\boldsymbol{\Omega}\cdot\mathbf{B}$ surface. Cheng *et al.* (1976) put their outer gap in the *open* magnetosphere, assuming the depleting perturbation to be the particle flux across the light cylinder. Now, in the open magnetosphere the charge density is not given by equation (2), which is obtained in the hypothesis of no net particle flux along the magnetic field lines, and a null charge surface must coincide with a magnetic field lines tube. So, the particle flux across the light cylinder does not remove the particles from the null charge surface and therefore cannot cause a vacuum gap to grow.

Let us now consider the geometry of the emitting magnetic field lines. It is assumed here that the radiation derives from the magnetic field lines in the vicinity of the surface dividing the open part from the close corotating part of the magnetosphere, and that different arrival phases correspond to the emission from regions at different radii from the star surface to the light cylinder, where the magnetic field lines diverge substantially. We consider here the simplified case of an orthogonal rotator with a dipolar magnetic field in the rotating frame. If we set $\phi=0$ for the phase of photons emitted from the star surface in the direction of the magnetic axis, as seen by an observer in the equatorial plane, the phase ϕ at which the observer sees a photon emitted along the last open magnetic field line at a radius x in units of light cylinder radius $r_L = c/\Omega$ is given by

$$2\pi\phi_1 = -\theta-\chi-\xi_1-x\cos(\xi_1+\chi) \quad \text{(leading edge)}$$
$$2\pi\phi_2 = \theta+\chi-\xi_2-x\cos(\xi_2-\chi) \quad \text{(trailing edge)} \tag{3}$$

where (see Fig. 1)

$$\theta = \arcsin\sqrt{x} \tag{4}$$

is the magnetic colatitude of the emission point,

$$\chi = \arctan\frac{\sqrt{x-x^2}}{2(1-x)} \tag{5}$$

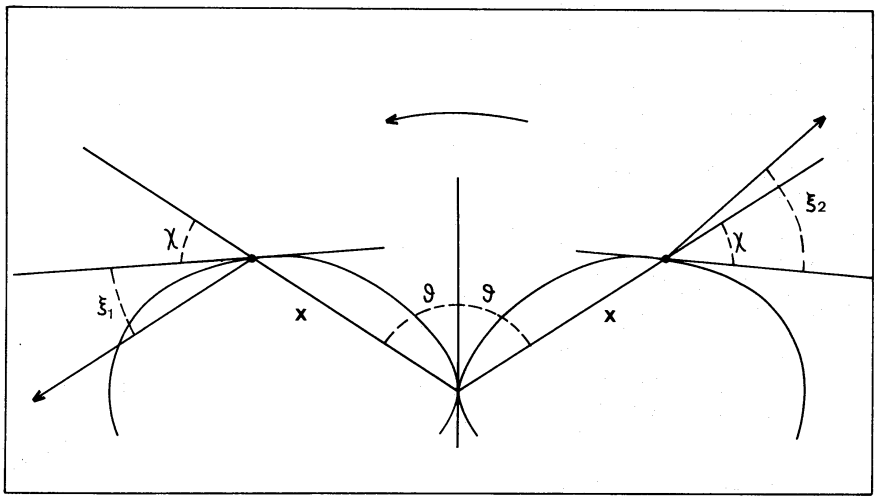

Figure 1. Emission field lines geometry. The curved arrow indicates the direction of rotation.

is the angle between the magnetic field line direction and the radial direction,

$$\xi_1 = \pi/2 - \chi - \arctan\left\{\frac{\cos\chi}{\gamma_R(x + \sin\chi)}\right\}$$

$$\xi_2 = \pi/2 + \chi - \arctan\left\{\frac{\cos\chi}{\gamma_R(x - \sin\chi)}\right\} \quad (6)$$

are the aberration angles for the emission on the leading and trailing edge, respectively, of the magnetosphere,

$$\gamma_R = (1 - x^2)^{-1/2} \quad (7)$$

is the Lorentz factor for the corotation motion and the last term

$$x\cos(\xi \pm \chi) \quad (8)$$

is the time delay due to the differences in the photon path lengths.

Fig. 2 shows the arrival phase ϕ of the photons deriving from the different radii between the star surface and the light cylinder. The two identical 0.5-phase shifted curves refer to the two different polar caps, the second being incomplete for clarity. The left-side branch of each curve represents the arrival phase for photons emitted along the leading edge of the open magnetosphere, while the nearly vertical right-side branches refer to the trailing edges. The radio, optical (Manchester *et al.* 1980) and gamma-ray (Kanbach *et al.* 1980) light curves of the Vela pulsar are superimposed on the arrival phase curves with the correct relative phase shifts. The zero levels for the three light curves have been located on purpose in coincidence with the $x = 0$, 0.5 and 0.7 values for the radio, optical and gamma-ray light curves, respectively, to show graphically that the first pulse optical and gamma-ray emissions likely arise near the leading edge of the open magnetosphere, about at the given $x = 0.5$ and $x = 0.7$ radii, respectively, the second pulse emission can be produced near the polar cap

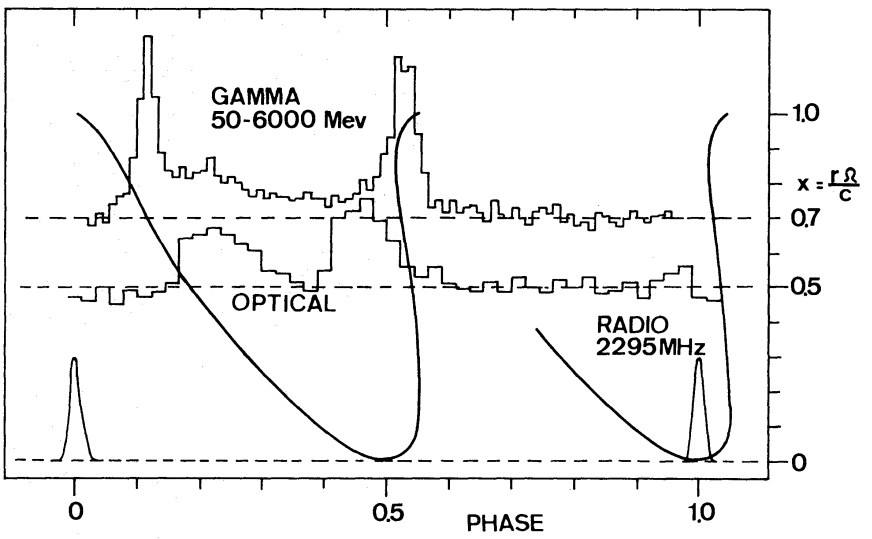

Figure 2. The Vela pulsar emission regions. The stressed curves represent the arrival phases of photons emitted tangentially to the last open magnetic field lines at different radii x between the star and the light cylinder (the curve relative to the second pole is incomplete for clarity). Superimposed are the radio, optical and gamma-ray light curves. An immediate interpretation of the figure is that the optical and gamma-ray emissions arise near the open magnetosphere edges, at a radius $x = 0.5$ and $x = 0.7$ respectively, while the radio pulse derives from the opposite polar cap, near the pulsar surface.

surface and everywhere in the vicinity of the trailing edge of the open magnetosphere, while the radio pulse derives from the opposite polar cap, near the pulsar surface. Moreover, the radiation observed in the region between the two pulses both in the gamma-ray and in the optical band can be produced by particles moving inside the open magnetosphere, at the same radius as the pulse emitting ones. The arrival phases ϕ in Fig. 2 have been calculated in the simplified case of an exactly orthogonal rotator with dipolar magnetic field. In a real situation we expect small distortions in the magnetic field from the dipolar configuration particularly in the light cylinder region (see for instance the Deutsch 1955 vacuum solution and the Endean & Allen 1970 low-density plasma solution), so there should be small differences between the expected and observed pulse phases, more in the gamma-ray than in the optical band.

Concluding, consideration of the light curves lead us to assume an emission scheme in which the first pulse optical radiation is produced about at $r = 0.5\, c/\Omega$ and the gamma-rays near $r = 0.7\, c/\Omega$, with the majority of the emission deriving from the magnetic field lines near the leading edge of the open magnetosphere, while the photons deriving from the polar cap surface and from the magnetic field lines near the trailing edge of the open magnetosphere join to give the second pulse emission.

3 Inverse Compton emission in the pulsar magnetosphere

The usual picture for the pulsar magnetosphere is considered in which electron–positron showers are produced near the polar cap surface in the photon interaction with the strong magnetic field. The details of the acceleration and pair creation mechanism can be either from Ruderman & Sutherland (1975) (for $\boldsymbol{\Omega}\cdot\mathbf{B}<0$ and large ion binding energy in the pulsar surface) or from Arons & Scharlemann (1979) or Jones (1980) (for $\boldsymbol{\Omega}\cdot\mathbf{B}>0$). As discussed in Morini (1981) within the Ruderman & Sutherland (1975) scheme the polar cap temperature is high enough in the case of the Vela pulsar ($T \simeq 3.5\times10^6$ K) to have copious gamma-ray emission from relativistic electrons ($\gamma = 10^2-10^5$) scattering thermal X-ray photons near the polar cap surface. The inverse Compton scattering with the overall star surface thermal emission ($T \simeq 10^6$ K) is found less important. In the Arons & Scharlemann (1979) scheme, instead, we have a lower polar cap temperature, while the scattering electrons are produced upwards in the magnetosphere, so that negligible inverse Compton emission results. Hereafter we put ourselves in the Ruderman & Sutherland (1975) scheme. The total particle luminosity for each polar cap is given by

$$L_p = 9.5\times10^{28} B_{12}^{6/7} R_6^3 \Omega^{15/7} \rho_6^{4/7} \text{ erg s}^{-1} \tag{9a}$$

($B_{12} = B_0/10^{12}$ G, etc.) with R the star radius and ρ the curvature radius of the field lines near the pulsar surface and the primary positron energy is

$$\gamma = 2.7\times10^6 B_{12}^{-1/7} \Omega^{1/7} \rho_6^{4/7} \tag{10a}$$

or more expediently

$$L_p = 2.1\times10^{30} B_{12}^{6/7} R_6^{23/7} \Omega^{13/7} (\rho/\rho_d)^{4/7} \text{ erg s}^{-1} \tag{9b}$$

$$\gamma = 6\times10^7 B_{12}^{-1/7} R_6^{2/7} \Omega^{-1/7} (\rho/\rho_d)^{4/7} \tag{10b}$$

where ρ_d is the minimum curvature radius for the field lines at the polar cap surface in the dipolar case

$$\rho_{d6} = 225\, R_6^{1/2} \Omega^{-1/2}. \tag{11}$$

As a result of magnetic photoabsorption the primary positrons are converted into electron–positron pairs with a broad energy distribution which we assume

$$N(\gamma) \propto \gamma^{-p} \tag{12}$$

with a maximum value for the energy of the order

$$\gamma = 2.7 \times 10^4 B_{12}^{-3/7} R_6^{5/14} \Omega^{1/14} (\rho/\rho_d)^{5/7}. \tag{13}$$

In the polar cap region these electrons scatter the thermal X-ray photons from the polar cap surface at a temperature

$$T = 8.2 \times 10^5 B_{12}^{1/4} \Omega^{1/4} \tag{14}$$

giving gamma-ray inverse Compton photons, as discussed in Morini (1981).

Following the suggestion of Hardee (1979) and Machabeli & Usov (1979), I suppose that these secondary electrons stream along the magnetic field lines with pitch angle reduced to zero by the decreasing magnetic field through the adiabatic invariance of the magnetic moment up to a radius r_0 where the relativistic particle energy density equals the magnetic field energy density. The value of r_0 depends on the energy content of the particle beam, on its shape and on the pulsar magnetic field, supposed here dipolar. With a simple algebra we find

$$r_0 = 0.57\ (k/k')^{-1/3} c/\Omega \tag{15}$$

where k is the ratio of the particle luminosity L_p (equation 9a) to the total energy loss (Deutsch 1955; Goldreich & Julian 1969)

$$L_T = \frac{2}{3} \frac{B_0^2 R^6 \Omega^4}{c^3} \tag{16}$$

and k' the surface fraction of the active polar cap $[R_c = R(R\Omega/c)^{1/2}]$ occupied by the relativistic beam.

At $r > r_0$ the growing plasma instability produces a substantial turbulent magnetic field δB, so that the particle trajectories are isotropically scattered within a cone of semi-aperture $\psi \simeq \delta B/B_\parallel$ around the dipolar configuration of the magnetic field. Also the particles acquire a non-zero pitch angle ζ. The numerical values for the angles ψ and ζ depend on the details of the plasma instability mechanism which are not yet well defined in the reference discussions. While we find a general agreement about a value $\delta B \simeq 0.1\ B_\parallel$ for the turbulent magnetic field (Hardee & Rose 1974; Benford 1975), for the pitch angle ζ the reported values range from $\zeta \sim 0.1$ (Hardee & Rose, 1974) to $\zeta < 10^{-2}$ (Benford 1975) and $\zeta \simeq 10^{-4}$ (Machabeli & Usov 1979). In the computer calculations whose results are presented in the next section the emission angle ψ and the pitch angle ζ have been considered arbitrary parameters and their values have been chosen to reproduce the observed spectrum of the Vela pulsar.

At a given height r within the beam one has a contribution of synchrotron photons deriving from all the radii r' between r_0 and r given by

$$\frac{dS_\nu}{dr'} = j_\nu(r') \frac{1 - \cos\alpha'}{1 - \cos\psi} \Big/ \cos[\chi(r') \pm \xi(r')] \tag{17}$$

where $\alpha' < \psi$ is the angular extent of the beam emission in r' as seen from r, the + or − signs are for the leading and trailing beam, respectively, and

$$j_\nu(r') = \epsilon_\nu(r') - \alpha_\nu(r') \int_{r_0}^{r'} j_\nu(r'')/\cos[\chi(r'') \pm \xi(r'')]\, dr'' \tag{18}$$

with ϵ_ν and α_ν the standard synchrotron emission coefficient (number of photons emitted in the unit time for unit volume element and frequency interval) and autoabsorption coefficient, respectively. The total synchrotron flux in r is the integral of (17)

$$S_\nu(r) = \int_{r_0}^{r} \frac{dS_\nu}{dr'}\, dr'. \tag{19}$$

The general formulae for inverse Compton scattering with an anisotropic photon field are derived in Morini (1981). In the case in which all the photons move in the same direction with an angle α with respect to the electron trajectory and with the same energy $\epsilon = h\nu$ the electron energy loss is given, for $\gamma \gg 1$, by

$$\left(\frac{dE}{dt}\right)_C = -n\epsilon c\, \sigma_{KN}(\epsilon') \frac{\gamma^2(1-\cos\alpha)^2}{1 + \dfrac{\gamma\epsilon}{mc^2}(1-\cos\alpha)} \tag{20}$$

where n is the photon density in the observer frame and $\sigma_{KN}(\epsilon')$ is the Klein–Nishina cross-section calculated for the photon energy ϵ' in the electron frame

$$\epsilon' = \gamma\epsilon(1 - \beta\cos\alpha). \tag{21}$$

The scattered photon energy ϵ_γ is given by

$$\epsilon_\gamma = \frac{\gamma^2\epsilon(1-\cos\alpha)}{1 + \dfrac{\gamma\epsilon}{mc^2}(1-\cos\alpha)}. \tag{22}$$

If instead the photons are isotropically distributed within a cone of semi-aperture $\alpha_0 > \gamma^{-1}$ around the electron direction, we have

$$\left(\frac{dE}{dt}\right)_C = -\frac{n\epsilon c}{1-\cos\alpha_0} \int_0^{\alpha_0} \sigma_{KN}(\epsilon') \frac{\gamma^2\epsilon(1-\cos\alpha)^2}{1 + \dfrac{\gamma\epsilon}{mc^2}(1-\cos\alpha)} \sin\alpha\, d\alpha \tag{23}$$

and

$$\epsilon_\gamma = \frac{\gamma^2\epsilon(1-\cos\alpha_0)}{\dfrac{3}{2} + \dfrac{\gamma\epsilon}{mc^2}(1-\cos\alpha_0)} \tag{24}$$

while the photon density n is related to the flux S_ν by the expression

$$n = \frac{4}{c}\frac{1-\cos\alpha_0}{1-\cos 2\alpha_0} S_\nu. \tag{25}$$

In the pulsar context the equations (20–25) must be used for the scattering both with the thermal photons from the polar cap surface and with the synchrotron photons in the light cylinder region. In our calculations equations (23) and (24) have been used in the case in which the angular aperture $\alpha'(r')$ of the photon cone deriving from r' is greater than the electron–photon average scattering angle $\alpha''(r')$ due to the curvature of the field line between r' and r

$$\alpha''(r') = \theta(r) + \chi(r) + \xi_1(r) - \theta(r') - \chi(r') - \xi_1(r') - \frac{\Omega}{c}\int_{r'}^{r} 1/\cos[\chi(r'') + \xi_1(r'')]\, dr'' \tag{26}$$

for the leading beam and a similar one for the trailing beam, with the integral in the second term accounting for the electron travel time from r' to r. Where $\alpha'' > \alpha'$, instead, equations (20–21) have been used. In both the cases $\alpha + \psi$ has been taken as scattering angle.

As we consider inverse Compton scattering with a continuum photon spectrum, both in the evaluation of the electron energy loss and of the emitted spectrum the contributions from the monoenergetic photon components must be integrated over the whole scattered photon spectrum, with an additional integration in the case of the synchro-Compton emission due to the different scattering angles for photons deriving from different radii r'. Through the set of equations (17–26) one can solve the energy equation for the electrons

$$\frac{dE}{dt} = \left(\frac{dE}{dt}\right)_S + \left(\frac{dE}{dt}\right)_C \tag{27}$$

where $(dE/dt)_S$ is the synchrotron energy loss, obtaining the particle energy distribution in the different points of the magnetosphere and simultaneously the emitted synchrotron and inverse Compton spectrum and, by means of the expressions (3), the light curves in the different energy bands. The set of equations described above has been numerically solved for different values for the pulsar parameters. In the next section the most relevant results for the Vela pulsar are presented.

4 The Vela pulsar

The results of computer calculation for the parameter values reported in Table 1 are shown in Figs 3–8. A few remarks are required. The values for the surface magnetic field ($B_0 = 5 \times 10^{12}$ gauss) and for the star radius ($R = 10^6$ cm) are consistent with the observed value for $L_T = I\Omega\dot{\Omega}$ assuming $I = 2 \times 10^{45}$ g cm^2 (see equation 16). The curvature radius for the

Table 1. Parameter set for the Vela pulsar model.

Surface magnetic field	$B_0 = 5 \times 10^{12}$ G
Neutron star radius	$R = 10^6$ cm
Angular velocity	$\Omega = 70\ s^{-1}$
Curvature of surface field lines	$(\rho/\rho_d) = 10$
Label of emission field lines	$n_f = 0.84$
Electron energy distribution	$N(\gamma) \propto \gamma^{-3}$
for	$1780 = \gamma_1 < \gamma < \gamma_2 = 31\,600$
Beam section/polar cap section	$k' = 0.00032$
Emission angle	$\psi = 0.7$ rad
Pitch angle	$\zeta = 5 \times 10^{-4}$ rad

surface magnetic field lines is supposed greater than in the dipolar case, to account for the observed gamma-ray luminosity within the Ruderman & Sutherland scheme, since the luminosity given by equation (9a) grows with the curvature radius of the field lines. It is assumed that the two field lines concerned with the electron beams (one near the leading edge and the other near the trailing edge of the open magnetosphere) are those lines labelled with $n_f = 0.84$, that is whose intersections with the star surface are at a distance 0.84 from the magnetic pole in polar cap radius units, on the rotation equator. This choice allows one to best reproduce the observed light curves. The value for the ratio k' between the beam section and the open magnetosphere section at the synchroton emission radius r_0 has been arranged to have $r_0 \simeq 0.5\, c/\Omega$ accordingly with equation (15) with the value for k given by the ratio between the particle luminosity L_p (equation 9a) and the total luminosity L_T (equation 16). The rather large value for the emission angle ($\psi = 0.7$ rad) is required both for reproducing the large pulses of the optical light curve in spite of the very small thickness of the synchrotron emission regions, and for the necessity to have large scattering angles for an efficient inverse Compton energy loss. Actually the growth with ψ^{-2} of the photon density along the electron trajectory for decreasing emission angles is widely exceeded by the ψ^4 dependence of the inverse Compton energy loss for small scattering angles.

The initial electron energy distribution $N(\gamma) \propto \gamma^{-3}$ between $\gamma_1 = 1780$ and $\gamma_2 = 31\,600$ is transformed by the inverse Compton energy loss with the thermal photons near the star surface into an energy distribution which can be described as $N(\gamma) \propto \gamma^{-2.75}$ between $\gamma_1' = 375$ and $\gamma_2' = 1670$ and $N(\gamma) \propto \gamma^{-2.35}$ between $\gamma_2' = 1670$ and $\gamma_3' = 16\,500$ and this energy distribution has been taken as input energy distribution for the synchro-Compton emission.

Fig. 3 presents the resulting emission spectrum. The prevalent emission mechanisms at the different energies are synchrotron in the optical and UV bands (from ~1 to 400 eV), thermal emission in the soft X-ray band (from 400 eV to 4 keV) from the hot polar cap surface which has a temperature $T = 3.7 \times 10^6$ K, inverse Compton scattering of the synchrotron photons in the hard X-ray and gamma-ray bands (from 4 keV to ~ 400 MeV) and inverse Compton scattering of the thermal photons in the high-energy gamma-ray band (from ~400 MeV to

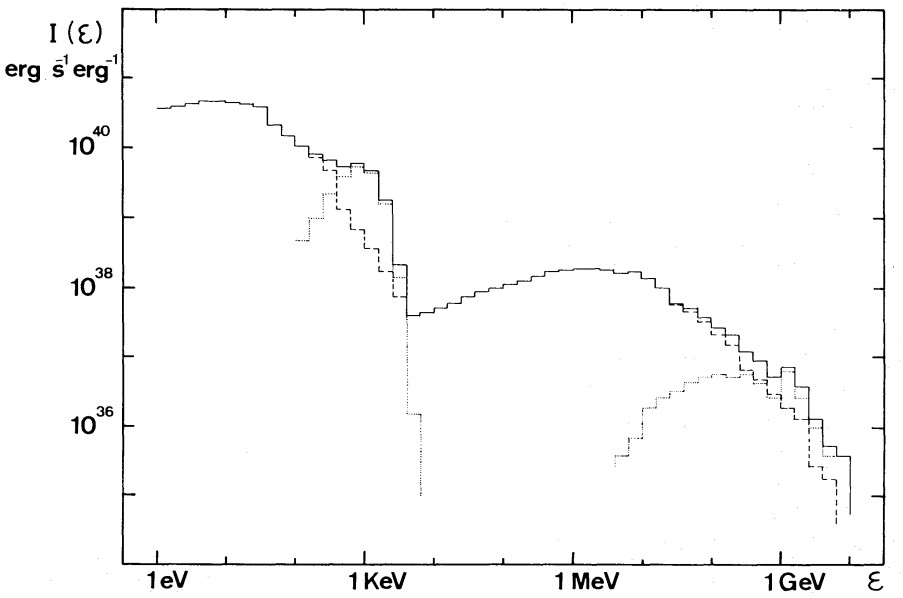

Figure 3. Total source spectrum. Dashed (– – –) is the synchron-Compton spectrum, dotted (· · · ·) the blackbody spectrum and the corresponding inverse Compton spectrum. The continuum line is the total spectrum.

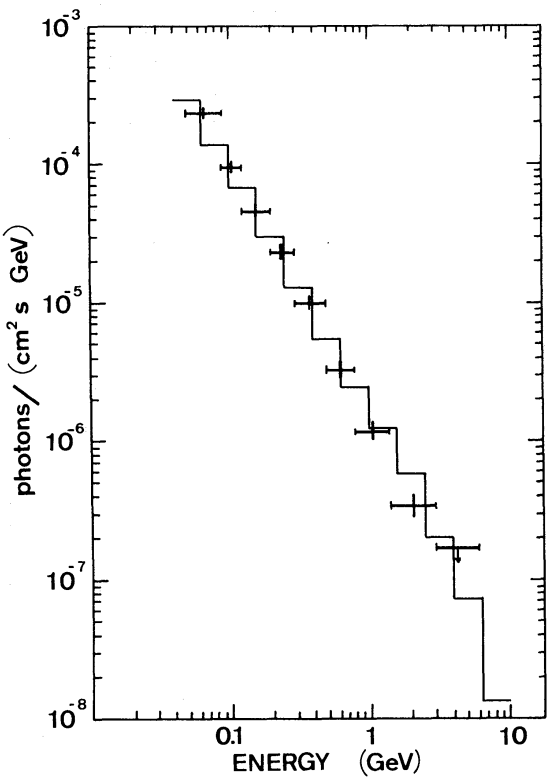

Figure 4. The gamma-ray photon spectrum after convolution with the *COS-B* energy resolution, compared with the *COS-B* Vela spectrum (crosses) from Kanbach *et al.* (1980).

~ 10 GeV). Assuming a distance $d = 500$ pc, an absorption $A_U = 0.7$ mag along the line-of-sight, and an optical duty cycle $f = 0.4$ consistent with the observed optical light curve, the synchrotron spectrum corresponds to an apparent magnitude $m_U = 23.4$ well in agreement with the mean pulsed apparent magnitude of the Vela pulsar $m_U = 23.8$ (Peterson *et al.* 1978).

The total gamma-ray spectrum is compared in Fig. 4 with the 50 MeV–6 GeV spectrum for the Vela pulsar observed by the *COS-B* satellite (Kanbach *et al.* 1980). A gamma-ray duty cycle $f = 0.105$ has been assumed. The photon spectrum presented in Fig. 4 is derived from the energy spectrum shown in Fig. 3, after convolution with the *COS-B* energy resolution which is ~ 60 per cent FWHM near 1 GeV (Scarsi *et al.* 1977). Fig. 5 shows the relative intensity of the second to the first gamma-ray pulse at different energies, compared with the corresponding data from the *COS-B* observations reported by Kanbach *et al.* (1980). Yet the computer results have been passed through the energy resolution of the *COS-B* detector to allow the comparison. The gamma-ray emission from the two pulses arises from different mechanisms, the first pulse being inverse Compton scattering of synchrotron photons near the light cylinder radius while the second one is partly inverse Compton scattering of synchrotron photons as the first one and partly inverse Compton scattering of thermal photons near the star surface. The thermal inverse Compton spectrum is harder than the synchro-Compton one (see Fig. 3), so the second pulse is stronger at higher energies.

Fig. 6 presents the light curves in the different energy bands. Since at the synchrotron emission radius ($r_0 = 0.5\, c/\Omega$) the relativistic beaming has not a relevant effect, in the optical-UV (1 – 100 eV) and X-ray (0.1–10 keV) bands the pulse width is essentially due to the angular distribution of the synchrotron emitting electrons within a cone of semi-aperture $\psi = 0.7$ rad. In the X-ray (0.1–10 keV) band the first pulse is flatter than in the optical

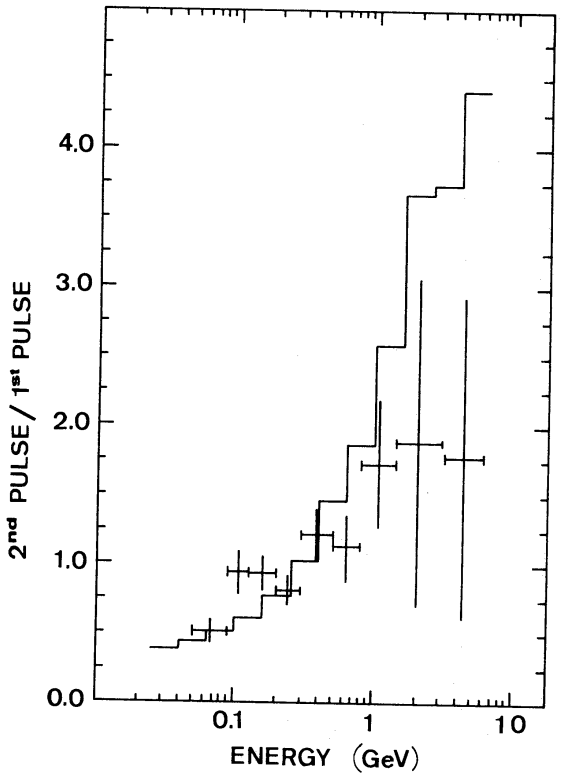

Figure 5. The expected second pulse/first pulse ratio compared with the *COS-B* data from Kanbach *et al.* (1980).

band. In fact, the X-ray synchrotron emission derives from a very thin region near r_0 where the more energetic electrons have not yet lost energy and the magnetic field is stronger. Optical synchrotron emission, instead, is produced in a wider region both by the less energetic electrons near r_0 and by the more energetic electrons upwards where the magnetic field is weaker, resulting in a pulse which is the sum of the emission at different heights with different relativistic beaming factors. In the X-ray band, moreover, the second pulse results as the superposition of synchrotron emission at r_0 and thermal blackbody emission from the star surface. At higher energies ($E > 10$ keV) the emission is inverse Compton scattering near the light cylinder radius and the pulse is narrowed by the strong relativistic beaming effect. The first pulse is also phase shifted with respect to the first optical pulse because it is emitted upwards, as already explained in Section 2. The different intensity of the two pulses can be easily explained. Since the magnetic field is dipolar in the corotating frame, in an inertial frame the leading field lines result rolled up while the trailing field lines are straight. The way from r_0 to the light cylinder is therefore longer along a leading field line than along the corresponding trailing field line, so that the electrons emit more synchrotron photons in the leading beam than in the trailing one, resulting in the first optical pulse being a little stronger than the second pulse. In the case of the inverse Compton emission the relative intensity of the two pulses is much greater than for the synchrotron emission. In fact, (i) within the leading beam the photon density is higher than in the trailing one because the first pulse synchrotron emission is stronger and (ii) the electrons travel more within the leading photon beam than in the trailing beam. In the high-energy gamma-ray band ($E > 50$ MeV) the second pulse is mainly inverse Compton emission near the star surface. The pulse is narrow because the emission is along the magnetic field lines deep in the magnetosphere before they spread out, and double peaked for the two beams distribution of the emitting electrons on the polar cap surface. The thermal inverse Compton emission appears in the 1–50 MeV light curve too as two small enhancements in the second pulse profile.

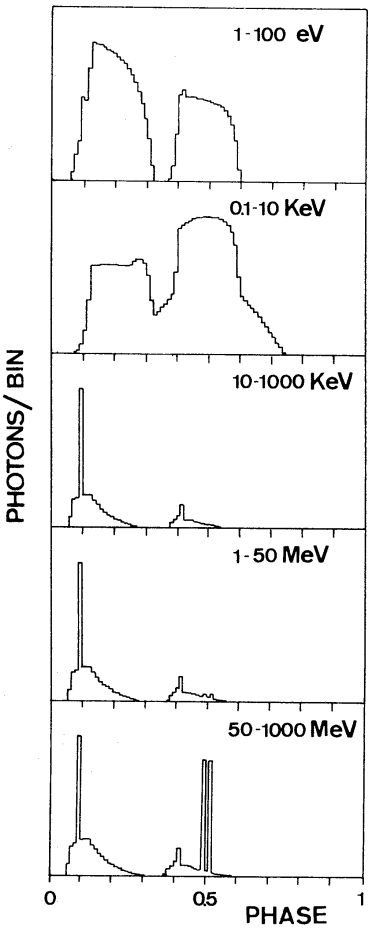

Figure 6. Expected light curves in the different energy band.

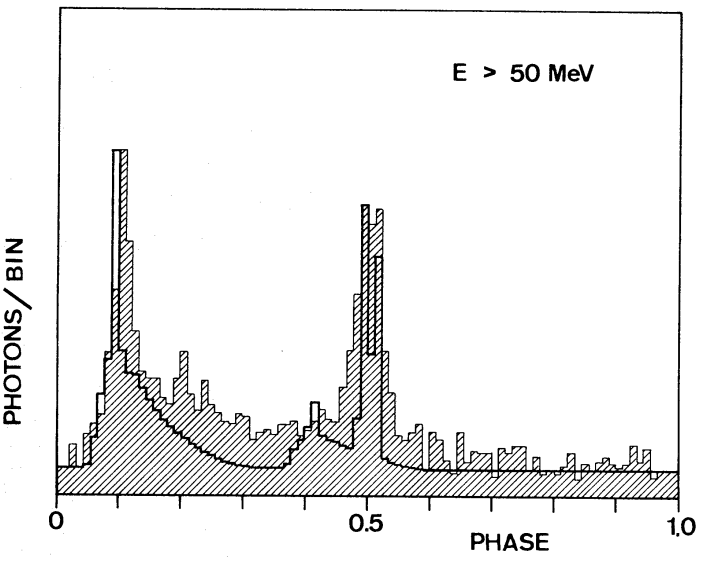

Figure 7. The expected gamma-ray light curve after convolution with the *COS-B* time resolution (stressed line), compared with the corresponding 90 bins *COS-B* light curve of the Vela pulsar (hatched zone) from Kanbach *et al.* (1980). The zero level for the expected light curve has been placed in coincidence with the background line of the *COS-B* light curve.

In Fig. 7 the gamma-ray light curve is compared with the 90 bins Vela pulsar light curve observed by the *COS-B* satellite (Kanbach *et al.* 1980). To allow the comparison the 1000 bins light curve resulting from the computer calculation has been convoluted with the temporal resolution of the *COS-B* light curve, which I have tentatively assumed 0.66 ms FWHM (Scarsi *et al.* 1977 estimates the *COS-B* uncertainty on photon arrival times better than 1 ms). The light curve so obtained has been compacted within 90 bins. The result has been to fill the hole between the two near peaks of the second pulse and a little smoothing of the first pulse shape.

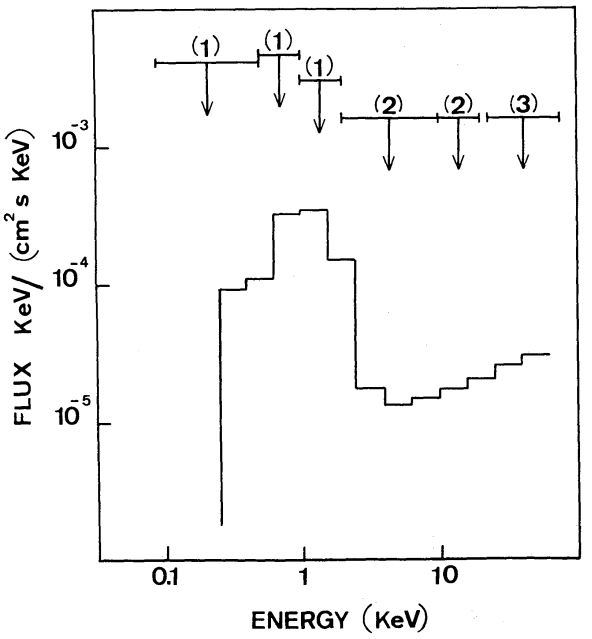

Figure 8. The expected pulsed X-ray spectrum compared with the upper limits from: (1) Zimmermann (1980), (2) Pravdo *et al.* (1976) and (3) Ricker *et al.* (1973). It has been assumed an absorbing column $N_H = 10^{21}\,cm^{-2}$ and a duty cycle $f = 0.4$ for $E < 4$ keV and $f = 0.1$ for $E > 4$ keV.

Finally, in Fig. 8 the X-ray spectrum is compared with the best available upper limits for the Vela pulsed X-ray fluxes (Zimmermann 1980; Pravdo *et al.* 1976; Ricker *et al.* 1973). An absorbing column $N_H = 10^{21}\,cm^{-2}$ has been assumed. Both the spectrum and the upper limits account for an X-ray duty cycle $f = 0.4$ for energies less than 4 keV and $f = 0.1$ for energies greater than 4 keV, in accord with the light curves reported in Fig. 6 and the spectrum in Fig. 3.

5 Discussion

It is unquestionable that the results presented about the gamma-ray emission of the Vela pulsar fit all the observational data collected up to date. Low-energy gamma-ray (~1 MeV) observations with the presently available instruments should be able to confirm the model, as it predicts that: (i) the $\sim E^{-2}$ photon spectrum observed in the high-energy-gamma-ray range bends at 10 MeV and becomes an E^{-1} photon spectrum in the 1 MeV region; (ii) the second pulse emission is practically suppressed at energy less than 50 MeV.

It should be of interest to look for a pulsed soft X-ray (~1 keV) blackbody emission from the hot polar cap. On the other hand a possible non-detection could be explained by the

masking effect produced by the steady thermal emission from the overall star surface. Furthermore, the thermal emission from the other polar cap could also be detected; in this case the pulsed feature of the polar cap radiation would be substantially reduced, as it can be realized considering the 0.1–10 keV light curve in Fig. 6, where the thermal radiation from one polar cap has been assumed.

The model can be used to estimate the optical and gamma-ray emission from slower pulsars. The most important difficulty in this line is that the result depends not only on the assumption of a few quantities which can be inferred from radio observations and from our present knowledge about the pulsar environment (such as for instance the value of the surface magnetic field B_0), but also on other free parameters (typically the beam to polar cap section ratio k', the emission angle ψ and the pitch angle ζ). It is necessary therefore to fix their values for the different pulsar frequencies Ω before applying the model to pulsars different than the Vela pulsar. A possibility which appears promising is to set a limit to the parameter freedom through a fitting to the Crab data, inferring their dependence on the period from the appropriate values for the Crab and Vela pulsars. The Crab pulsar, however, presents a variety of differences with respect to the Vela pulsar (for instance the sharpness of the optical pulses which might be due to coherent emission and the two radio pulses coincident with the optical, X- and gamma-ray pulses), so that the problem to force the Crab and Vela pulsars within the same model is not easy.

The problem of the dependence of the gamma-ray pulsar luminosity on the period and age is also of importance for the understanding of the nature of the unidentified gamma-ray point sources detected by the *COS-B* satellite. It has been shown, in fact, that the observed gamma-ray sources distribution can be easily explained by means of pulsars if these emit gamma-rays during an active gamma-ray lifetime of the order 3×10^4 yr with a power-law dependence of the gamma luminosity on the pulsar age consistent with the Crab and Vela data (Buccheri, Morini & Sacco 1981). On this line it is of interest also to note that in the case of the Vela pulsar the model explains the emission in the radio band and in the optical to gamma-ray band through two quite independent radiation mechanisms in different magnetosphere regions. It could be expected, therefore, that a few gamma-ray sources are pulsars not detected in the radio band both because they are radio silent or because the radio emission is beamed in a different direction from the gamma-rays.

Acknowledgments

I wish to thank Professor L. Scarsi, Dr R. Buccheri and Dr A. Treves for useful suggestions and discussions.

References

Arons, J. & Scharlemann, E. T., 1979. *Astrophys. J.*, **231**, 854.
Ayasli, S., 1981. *Astrophys. J.*, **249**, 698.
Ayasli, S. & Ögelman, H. B., 1980. *Astrophys. J.*, **237**, 227.
Benford, G., 1975. *Astrophys. J.*, **201**, 419.
Bennett, K., Bignami, G. F., Boella, G., Buccheri, R., Hermsen, W., Kanbach, G., Lichti, G. G., Masnou, J. L., Mayer-Hasselwander, H. A., Paul, J. A., Scarsi, L., Swanenburg, B. N., Taylor, B. G. & Wills, R. D., 1977. *Astr. Astrophys.*, **61**, 279.
Buccheri, R., 1981. *Pulsars, IAU Symp. No. 95*, p. 241.
Buccheri, R., Caraveo, P., D'Amico, N., Hermsen, W., Kanbach, G., Lichti, G. G., Masnou, J. L., Wills, R. D., Manchester, R. N. & Newton, L. M., 1978. *Astr. Astrophys.*, **69**, 141.
Buccheri, R., Morini, M. & Sacco, B., 1981. *Phil. Trans. R. Soc. Lond. A*, **301**, 495.
Cheng, A. F. & Ruderman, M. A., 1977. *Astrophys. J.*, **216**, 865.

Cheng, A. F., Ruderman, M. A. & Sutherland, P. G., 1976. *Astrophys. J.*, **203**, 209.
Davila, J., Wright, C. & Benford, G., 1980. *Astrophys. Space Sci.*, **71**, 51.
Deutsch, A. J., 1955. *Ann. Astrophys.*, **18**, 1.
Endean, V. G. & Allen, J. E., 1970. *Nature*, **228**, 348.
Goldreich, P. & Julian, W. H., 1969. *Astrophys. J.*, **157**, 869.
Hardee, P. E., 1977. *Astrophys. J.*, **216**, 873.
Hardee, P. E., 1979. *Astrophys. J.*, **227**, 958.
Hardee, P. E. & Rose, W. K., 1974. *Astrophys. J.*, **194**, L35.
Harding, A. K., 1981. *Astrophys. J.*, **245**, 267.
Holloway, N. J., 1973. *Nature Phy. Sci.*, **246**, 6.
Jones, P. B., 1980. *Mon. Not. R. astr. Soc.*, **192**, 847.
Kanbach, G., Bennett, K., Bignami, G. F., Buccheri, R., Caraveo, P., D'Amico, N., Hermsen, W., Lichti, G. G., Masnou, J. L., Mayer-Hasselwander, H. A., Paul, J. A., Sacco, B., Swanenburg, B. N. & Wills, R. D., 1980. *Astr. Astrophys.*, **90**, 163.
Lichti, G. G., Buccheri, R., Caraveo, P., Gerardi, G., Hermsen, W., Kanbach, G., Masnou, J. L., Mayer-Hasselwander, H. A., Paul, J. A., Swanenburg, B. N. & Wills, R. D., 1980. *Advances in Space Exploration*, Vol. 7, Pergamon Press, Oxford.
Machabeli, G. Z. & Usov, V. V., 1979. *Pis'ma V. Astr. Zh.*, **5**, 445.
Manchester, R. N., Wallace, P. T., Peterson, B. A. & Elliott, K. H., 1980. *Mon. Not. R. astr. Soc.*, **190**, 9P.
Mandrou, P., Vedrenne, G. & Masnou, J. L., 1980. *Nature*, **287**, 124.
Massaro, E. & Salvati, M., 1979. *Astr. Astrophys.*, **71**, 51.
Massaro, E., Salvati, M. & Buccheri, R., 1979. *Mon. Not. R. astr. Soc.*, **189**, 823.
Mestel, L., 1971. *Nature Phy. Sci.*, **233**, 149.
Morini, M., 1981. *Astrophys. Space Sci.*, **79**, 203.
Newton, L. M., Manchester, R. N. & Cooke, D. J., 1981. *Mon. Not. R. astr. Soc.*, **194**, 841.
Ögelman, H., Fichtel, C. E., Kniffen, D. A. & Thompson, D. J., 1976. *Astrophys. J.*, **209**, 584.
Peterson, B. A., Murdin, P., Wallace, P., Manchester, R. N., Penny, A. J., Jorden, A., Hartley, K. F. & King, D., 1978. *Nature*, **276**, 475.
Pinkau, K., 1979. *Nature*, **277**, 17.
Pravdo, S. H., Becker, R. H., Boldt, E. A., Holt, S. S., Rothschild, R. E., Serlemitsos, P. J. & Swank, J. H., 1976. *Astrophys. J.*, **208**, L67.
Radhakrishnan, V. & Cooke, D. J., 1969. *Astrophys. Lett.*, **3**, 225.
Ray, A. & Benford, G., 1981. *Phy. Rev. D*, **23**, 2142.
Ricker, G. R., Garassimenko, M., McClintock, J. E., Ryckman, S. G. & Lewin, W. G. H., 1973. *Astrophys. J.*, **186**, L111.
Ruderman, M. A. & Sutherland, P. G., 1975. *Astrophys. J.*, **196**, 51.
Salvati, M. & Massaro, E., 1978. *Astr. Astrophys.*, **67**, 55.
Scarsi, L., Bennett, K., Bignami, G. F., Boella, G., Buccheri, R., Hermsen, W., Koch, L., Mayer-Hasselwander, H. A., Paul, J. A., Pfeffermann, E., Stiglitz, R., Swanenburg, B. N., Taylor, B. G. & Wills, R. D., 1977. *Proc. 12th ESLAB Symp., Frascati, ESA Sp-124*, p. 3.
Schlickeiser, R., 1980. *Astrophys. J.*, **236**, 945.
Shen, C. S., 1972. *Phys. Rev. D*, **6**, 2736.
Swanenburg, B. N., Bennett, K., Bignami, G. F., Buccheri, R., Caraveo, P., Hermsen, W., Kanbach, G., Lichti, G. G., Masnou, J. L., Mayer-Hasselwander, H. A., Paul, J. A., Sacco, B., Scarsi, L. & Wills, R. D., 1981. *Astrophys. J.*, **243**, L69.
Thompson, D. J., 1975. *Astrophys. J.*, **201**, L117.
Wallace, P. T., Peterson, B. A., Murdin, P. G., Danzinger, I. J., Manchester, R. N., Lyne, A. G., Goss, W. M., Smith F. G., Disney, M. J., Hartley, K. F., Jones, D. H. P. & Wellgate, G. B., 1977. *Nature*, **266**, 692.
Zheleznyakov, V. V. & Shaposhnikov, V. E., 1972. *Astrophys. Space Sci.*, **18**, 166.
Zimmermann, H. U. 1980. *Astr. Astrophys.*, **88**, 309.